Pressure-Optimized Band Gap and Enhanced Photoelectric Response of Graphitic Carbon Nitride with Nitrogen Vacancies

Peng Cheng,[1,2] Deyuan Yao,[1,2] Jinwei Yan,[1,2] Tingting Ye,[1,2] Huanhuan Liu,[3] Hong Zeng,[1,2] Xiaomei Pan,[1,2] Genqiang Zhang,[3,*] and Junfeng Ding[1,2,4,†]

[1] *Key Laboratory of Materials Physics, Institute of Solid State Physics, Hefei Institutes of Physical Science, Chinese Academy of Sciences, Hefei 230031, China*

[2] *Science Island Branch, Graduate School of USTC, Hefei 230026, China*

[3] *CAS Key Laboratory of Materials for Energy Conversion, Department of Materials Science and Engineering, University of Science and Technology of China, Hefei 230026, China*

[4] *Jianghuai Frontier Technology Coordination and Innovation Center, Hefei 230088, China*

(Received 19 July 2022; revised 8 December 2022; accepted 27 January 2023; published 16 February 2023)

Graphitic carbon nitride (g-C_3N_4) shows favorable performance as a photocatalyst and has attracted widespread attention in recent years. As its wide band gap of 2.70 eV limits light absorption in the visible range, many efforts have been made to optimize the band gap. In this report, pressure is used to engineer the band gap and photoelectric response of nitrogen-deficient g-C_3N_4 nanoflakes. The band gap of the sample is first narrowed to 2.40 eV due to the introduction of nitrogen vacancies and then further narrowed to 1.70 eV by pressure, which is the lowest value reported in the literature for undoped g-C_3N_4. Accordingly, the photoelectric response increases by nearly 50% because of the enhanced light absorption at high pressure. More interestingly, after depressurization to ambient pressure, the optimized band gap survives with a minimum value of 1.87 eV accompanied by enhanced photoelectric responsivity. *In situ* synchrotron x-ray diffraction and Raman spectra suggest that the tunable band gap originates from irreversible pressure-induced amorphization with the assistance of vacancies for g-C_3N_4. The collaborative approach of introducing deficiency and pressure treatment adopted here shows the ability to engineer the band gap continuously over a prominently wider region than that for the single band-gap-narrowing technique, and thus, enhances the photoelectric performance for broadened semiconductors.

DOI: 10.1103/PhysRevApplied.19.024048

I. INTRODUCTION

Graphitic carbon nitride (g-C_3N_4) has attracted widespread attention in recent years owing to its favorable performance for efficient photocatalytic hydrogen generation, water oxidation, artificial photosynthesis, CO_2 reduction, photodecomposition of organic pollutants, and so on [1–14]. Band-gap engineering of g-C_3N_4 could significantly enhance its photocatalytic activity, as the wide band gap of 2.7 eV for pristine g-C_3N_4 limits light absorption in the visible range [15–21]. A series of experiments were carried out to narrow the band gap of g-C_3N_4, such as doping with nonmetallic or metallic elements [22–26], homogeneous amorphization [18], sensitization with dyes [27,28], and introducing point defects or vacancies [19,29–34]. Recently, nitrogen-deficient g-C_3N_x was successfully synthesized by alkali assistance with a tunable band gap ranging from 2.36 to 2.68 eV, which displayed enhanced photoelectric responsivity with prominent photocatalytic hydrogen performance [29]. To improve the application of g-C_3N_4, it is an irresistible trend to discover approaches to tuning the band gap of g-C_3N_4 continuously over a wide region.

Pressure, as a thermodynamic parameter, is a versatile tool for controlling the properties of materials by reducing interatomic distances and modifying electronic orbitals and bonding patterns. Thus, a high-pressure technique provides an effective strategy for a route to tune the band gap and photoelectric properties without the involvement of composition change [35–42]. Recently, pressure treatment has attracted growing interest to tune the electronic band structure of materials to optimize their photoelectric properties for various applications [43–50]. For example, the optimized band gap for single-junction solar cells in lead-based perovskites is achieved by narrowing the band gap of formamidinium lead triiodide [$HC(NH_2)_2PbI_3$] from 1.489 to 1.337 eV with a modest hydraulic pressure up to 2.1 GPa [51]. Although the pressure-optimized band structure and optical properties are abundantly reported

*gqzhangmse@ustc.edu.cn
†junfengding@hotmail.com

for various materials, investigations on the photoelectric properties to evaluate their performance for applications as photocatalysts, solar cells, photodetectors, and so on are lacking. Furthermore, because of the elastic stretch of the lattice under pressure, the pressure-driven modulations of the band gap are commonly reversible, and most of the optimized properties cannot be retained at ambient pressure due to dynamic instabilities.

Earlier theoretical efforts on the structural stability of g-C_3N_4 under pressure predicted the transition from g-C_3N_4 to superhard cubic C_3N_4 at approximately 12 GPa [52,53]. However, high-pressure experiments show that the lattice of g-C_3N_4 maintains the hexagonal structure with the $P63/m$ phase in the studied range up to 25 GPa [54]. A recent study investigated the pressure-modulated photoluminescence of g-C_3N_4 and reported a redshift of the center wavelength from blue (434 nm) to yellow (550 nm) at elevated pressures up to 15 GPa without a structural phase transition [55]. These results imply that pressure may be able to efficiently optimize the band gap and photoelectric properties of g-C_3N_4, which need to be further clarified.

Here, the band gap and photoelectric responsivity under pressure are systemically investigated in nitrogen-deficient g-C_3N_4 nanoflakes with a N : C ratio of 9 : 10. The pressure-optimized band gap enhances the visible-light absorption of nitrogen-deficient g-C_3N_4, which leads to a prominent increase in the photocurrent. Furthermore, with the assistance of nitrogen vacancies, irreversible pressure-induced amorphization appears with an optimized band gap and photoelectric responsivity under ambient conditions. Our results highlight that irreversible pressure-induced amorphization offers an opportunity to engineer the band gap for ambient-pressure applications.

II. EXPERIMENT

A. Synthesis of nitrogen-deficient g-C_3N_4

Nitrogen-deficient g-C_3N_4 nanoflakes with nitrogen-vacancy defects are synthesized by an alkali-assisted thermopolymerization process, according to a previous report [29]. In a typical procedure, 15 g of urea and 0.01 g of KOH are thoroughly ground in a mortar in a glove box under an Ar atmosphere. The mixtures are calcined at 550 °C in a muffle furnace for 4 h at a heating rate of 10 °C min^{-1}. The product is washed with distilled water at least 3 times to remove any residues and finally dried in a vacuum oven at 70 °C for 12 h.

B. *In situ* investigations under pressure

A high-pressure experiment is conducted with diamond anvil cells (DACs), which have two opposing diamonds producing high pressures with a culet size of 300 μm [56]. A central hole 200 μm in diameter is drilled in a T301 stainless-steel or rhenium (Re) gasket as the sample chamber. Nitrogen-deficient g-C_3N_4 samples are loaded into the chamber together with ruby powder to calibrate the pressure. Liquid silicon oil is adopted as the pressure-transmitting medium (PTM) in the Raman, PL, absorption spectra, and X-ray diffraction (XRD) measurements. For the high-pressure photocurrent experiments, we use cubic boron nitride as both the insulating layer and the PTM.

Incident laser wavelengths of 532 nm (for Raman measurements) and 488 nm (for PL measurements) are adopted for optical measurement by a backscattering geometry. The pressure is controlled through the four loading DAC screws. A single-stage imaging spectrograph, SP2500 (Acton), with a focal length of 500 mm is used to observe conditions inside the sample chamber, and optical signals are collected by a thermoelectrically cooled CCD detector array (Princeton eXcelon) simultaneously. The Raman and PL spectra record both compression and decompression processes of nitrogen-deficient g-C_3N_4 at selected pressures. The initial pressure is 0 GPa; here, it goes from 0 to 47.6 GPa through compression and then decreases back to ambient pressure. To extract the peak position in the PL spectra and Raman spectra, the Lorentzian function is adopted to fit experimental data.

The absorption spectra are detected by the system aforementioned, and the sample is loaded in the gasket with prepressing to a thickness of 10 μm to minimize changes in sample thickness after compression. A focused tungsten light source with wavelengths ranging from 400 to 1000 nm is used as the incident light to cross the diamond anvils, and the same chamber without sample is prepared as the control group.

High-pressure photocurrent measurements of nitrogen-deficient g-C_3N_4 are performed in a diamond anvil cell with 300 μm culets. A central hole with a diameter of approximately 300 μm is drilled in T301 stainless steel and then filled with cubic boron nitride (c-BN). c-BN is compressed as a gasket to achieve electrical insulation conditions between platinum (Pt) leads and a T301 stainless-steel gasket. Photoelectric measurements are conducted using a two-probe method, with the Pt heads touching the sample and the tail connected out. I-t data are recorded using a source meter (Keithley 2635B) at a bias of 15 V.

In situ high-pressure angle-dispersive synchrotron XRD experiments are carried out at the BL15U1 beamline of the Shanghai Synchrotron Radiation Facility (SSRF) and the 4W2 beamline of the Beijing Synchrotron Radiation Facility (BSRF). The incident wavelength of the monochromatic beam is 0.6199 Å, and the diameter of the spot size is approximately 10 μm. The sample-to-detector distance and the image-plate orientation angles are calibrated using the CeO_2 standard. All the XRD patterns are integrated to give one-dimensional powder diffraction patterns using the FIT2D program [57,58].

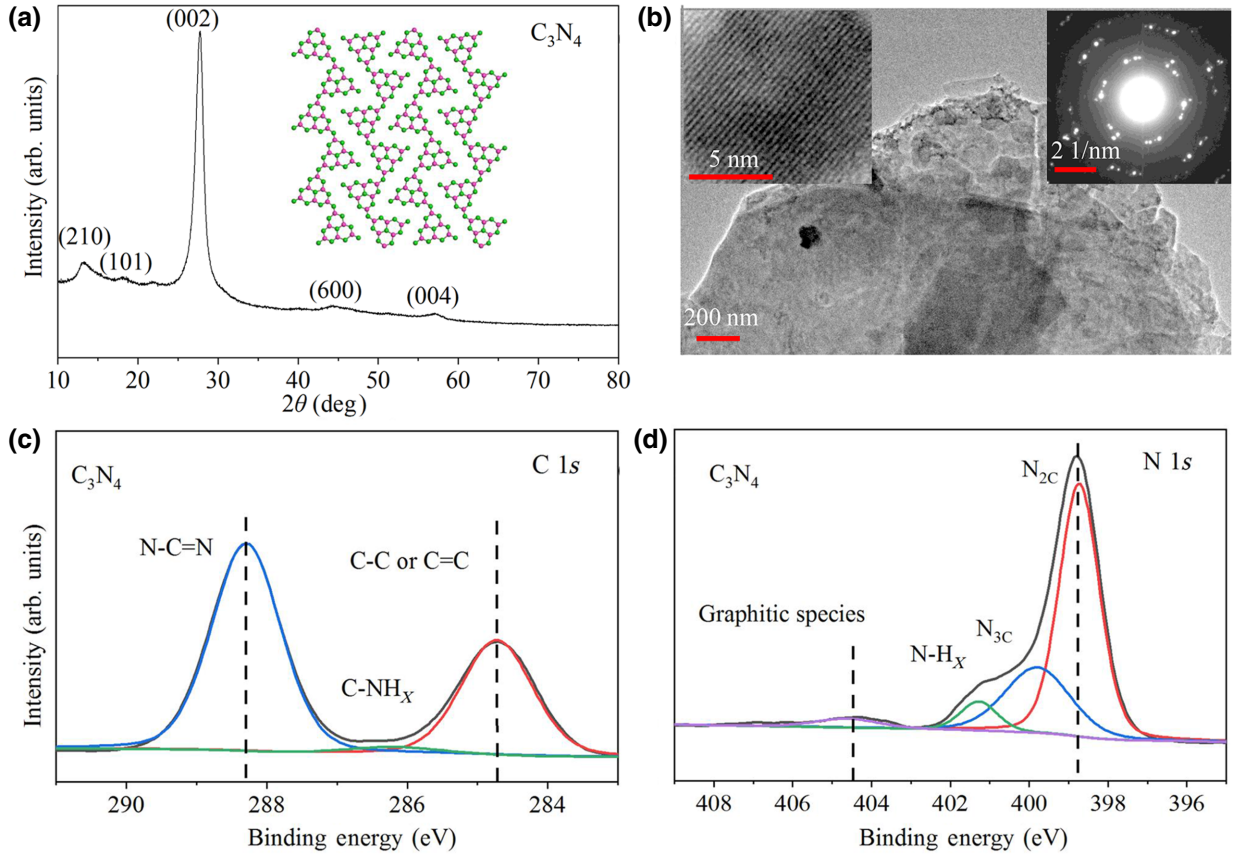

FIG. 1. Microstructural information of nitrogen-deficient g-C_3N_4 under ambient conditions. (a) XRD pattern and (b) TEM image of nitrogen-deficient g-C_3N_4. Inset shows a high-resolution TEM image and electron-diffraction pattern. (c) C 1s and (d) N 1s XPS spectra of nitrogen-deficient g-C_3N_4.

III. RESULTS AND DISCUSSION

A. Characterization of nitrogen-deficient g-C_3N_4 samples under ambient conditions

The morphology and chemical structure of nitrogen-deficient g-C_3N_4 are characterized by XRD, field transmission electron microscopy (TEM), and x-ray photoelectron spectroscopy (XPS) under ambient conditions, as shown in Fig. 1. The diffraction pattern in Fig. 1(a) is in good accordance with the XRD studies on g-C_3N_4 reported in the literature [59]. Two major reflections are observed at approximately $2\theta = 12.8°$ and $2\theta = 27.7°$. As the fully polymerized form of g-C_3N_4, characterized by a C : N ratio of 0.75, cannot be practically obtained, the material usually presents a hydrogen content and forms various polymorphs of g-C_3N_4 [14,60]. Suter *et al.* reported that different C : N : H ratios could exist in graphitic carbon nitride materials with tunable physical properties [14]. An earlier neutron-diffraction study suggested that the parallel chains of tri-s-triazine units organized in layers with an A-B stacking motif could fit the XRD experimental observations well [59]. According to earlier reports, the major reflections in Fig. 1(a) can be assigned to the (201) and (002) reflections of the orthorhombic geometry, respectively. A planar schematic diagram of the crystal structure for nitrogen-deficient g-C_3N_4 is exhibited in Fig. 1(a).

The TEM image in Fig. 1(b) indicates that nitrogen-deficient g-C_3N_4 retains the layered and sheet structure, which is similar to pristine g-C_3N_4. The high-resolution dark-field image shows that the thin regions at the sample edges reveal lattice fringes and layering representative of crystalline material with a graphitic structure. The electron-diffraction pattern shows the in-plane hexagonal geometry with interfacial stacking of nitrogen-deficient g-C_3N_4 nanoflakes. The XRD diffraction and TEM images confirm that the synthesized sample adopts a graphenelike two-dimensional layered structure.

To further explore the influence of N defects on the elemental composition and structure of nitrogen-deficient g-C_3N_4, XPS is performed. XPS data in Fig. S1 within the Supplemental Material [61] show a N : C ratio near 9 : 10, which is much lower than that of the original g-C_3N_4 (∼1.33), indicating that N defects are successfully introduced. The high-resolution spectra of C 1s and N 1s core electrons are depicted in Figs. 1(c) and 1(d), respectively. The C 1s XPS spectrum can be divided into

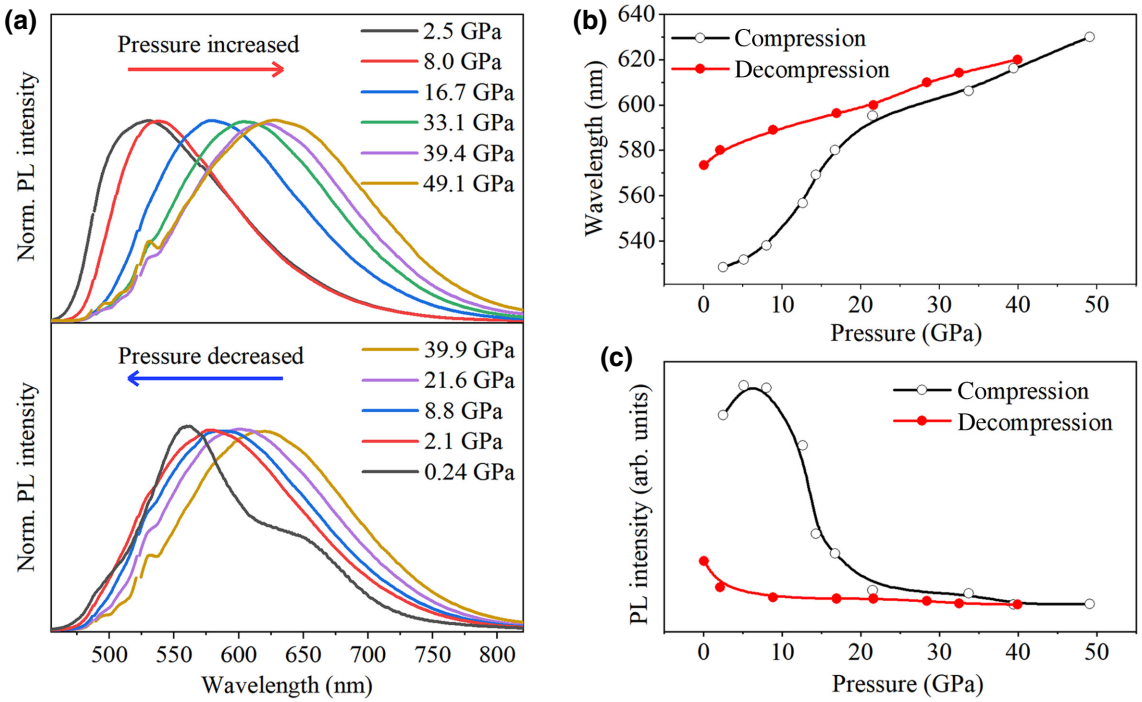

FIG. 2. Photoluminescence spectra for nitrogen-deficient g-C_3N_4 (488-nm excitation at room temperature) under pressure. (a) Normalized PL spectra of nitrogen-deficient g-C_3N_4 with increasing and decreasing pressure. (b) Wavelength shift and (c) intensity variation of the PL peaks during compression and decompression.

three peaks located at 288.3, 286.4, and 284.7 eV, which are associated with N-C=N coordination in the framework of nitrogen-deficient g-C_3N_4, C-NH_x ($x = 1$, 2) on the edges of heptazine units, and adventitious hydrocarbons, respectively [29]. The deconvolution of the N 1s spectrum contains three peaks centered at 398.7, 399.8, and 401.2 eV, which are assigned to bicoordinated (N_2C), tricoordinated (N_3C), and NH_x groups in the heptazine framework [29], while the peak at 404.4 eV corresponds to graphitic species [62]. XPS data support that the general structure of nitrogen-deficient g-C_3N_4 is preserved well together with the formation of N defects.

B. Pressure-optimized band gap of nitrogen-deficient g-C_3N_4

The color change for nitrogen-deficient g-C_3N_4 upon compression in Fig. S2 within the Supplemental Material [61] directly demonstrates the pressure-modulated optical properties. Upon compression, the color of nitrogen-deficient g-C_3N_4 changes from the initial faint yellow to totally red. After pressurized treatment, deep orange is preserved for nitrogen-deficient g-C_3N_4 at ambient pressure, as shown in Fig. S2(b) within the Supplemental Material [61]. In Fig. 2, the photoluminescence (PL) of nitrogen-deficient g-C_3N_4 under pressure is investigated. The small peaks at approximately 532 nm originate from the incident laser with wavelengths of 532 nm used for the Raman measurements. Although the 532-nm laser is blocked during the PL measurements, diffuse light still results in a noisy background in the PL spectra. The center wavelength of PL shows a shift from about 528 to 630 nm as the pressure increases from 2.5 to 49.1 GPa in Fig. 2(a), implying a narrowed band gap due to lattice shrinkage under pressure. The PL peak remains at 573 nm upon unloading to ambient pressure. The differences in both the center wavelength and intensity of PL between compression and decompression are noticeable, as shown in Figs. 2(b) and 2(c). The PL shift shows a kink with a prominent drop in intensity at approximately 17 GPa upon compression, while they change monotonically during depressurization. As the photoluminescence property is closely related to the electron structure, it is reasonable to assume that the pressure modulates the band gap of nitrogen-deficient g-C_3N_4.

To precisely determine the electronic band gap of nitrogen-deficient g-C_3N_4 under pressure, *in situ* UV-visible absorption spectroscopy is performed. Figures 3(a) and 3(b) show the ultraviolet-to-visible (UV-vis) diffuse reflectance spectra (DRS) and calculated band gaps for nitrogen-deficient g-C_3N_4 at selected pressures, respectively. Band gaps of the sample are determined by analysis using the transformed Kubelka-Munk function versus the energy of light absorbed. The initial nitrogen-deficient g-C_3N_4 sample at 0 GPa possesses a band gap of 2.40 eV, which is near the value of 2.36 eV reported in the

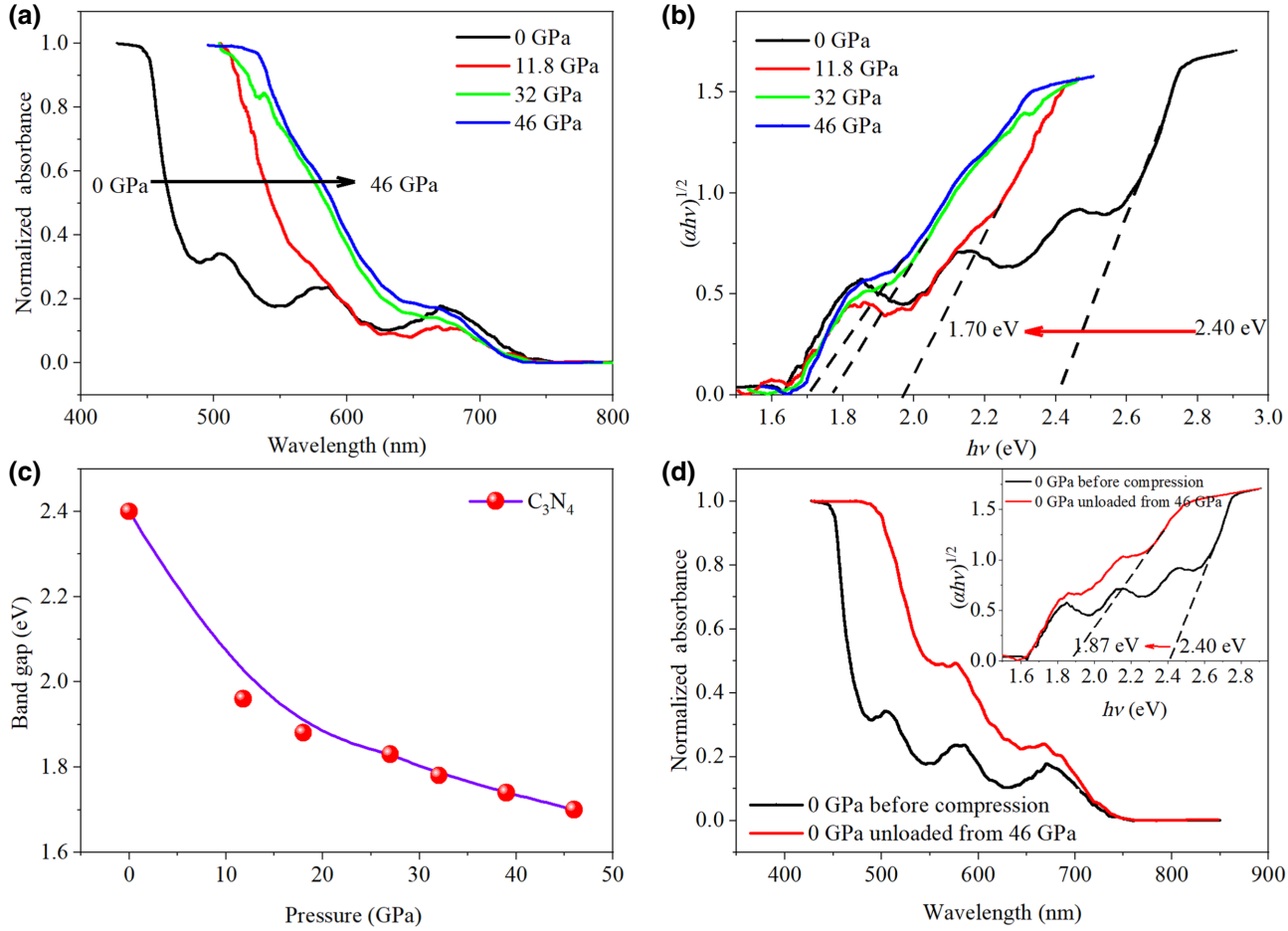

FIG. 3. (a) UV-vis DRS and (b) plots of the transformed Kubelka-Munk function versus photon energy for nitrogen-deficient g-C_3N_4 at elevated pressures (ranging from 0 to 46 GPa). (c) Pressure-dependent band gap of nitrogen-deficient g-C_3N_4 upon compression. (d) Comparison of UV-vis DRS spectra for nitrogen-deficient g-C_3N_4 at ambient pressure (before and after compression) and plots of the transformed Kubelka-Munk function versus photon energy (inset).

literature [29]. As the applied pressure increases, the light-absorption edge of the sample shows a significant redshift, and a minimum band gap of 1.70 eV is achieved at 46 GPa, which is the lowest value reported for g-C_3N_4. In Fig. 3(c), the band gap of nitrogen-deficient g-C_3N_4 is gradually narrowed upon compression with a kink at approximately 17 GPa, in accordance with the pressure-dependent PL in Fig. 2. The sample that undergoes the compression and decompression process from 0 GPa → 46 GPa → 0 GPa has a band gap of 1.87 eV, as shown in Fig. 3(d). Both PL and absorption spectroscopy indicate that pressure can efficiently narrow the band gap of nitrogen-deficient g-C_3N_4.

C. Pressure-enhanced photoelectric response of nitrogen-deficient g-C_3N_4

As the band gap dominates the light absorption of the semiconductor, the photocurrent of nitrogen-deficient g-C_3N_4 under pressure is investigated to evaluate the influence of the pressure-narrowed band gap on its photoelectric applications. Figure 4(a) sketches the experimental setup of the photocurrent measurements under pressure. The linear I-V curve in Fig. S3 within the Supplemental Material [61] shows the ohmic contact between the Pt electrodes and nitrogen-deficient g-C_3N_4 samples. In Figs. 4(b) and 4(c), the photocurrent under white light shows a considerable enhancement from 18 nA at 0 GPa to 29 nA at 17 GPa. With further increasing pressure up to 49 GPa, the photocurrent almost does not change. In accordance with the retained band gap upon decompression in Fig. 3, the pressure-enhanced photocurrent can be retained at ambient pressure with a value of approximately 30 nA in Fig. 4(c) and Fig. S4 within the Supplemental Material [61]. The pressure dependence of the photocurrent implies that pressure can efficiently optimize the photoelectric application of nitrogen-deficient g-C_3N_4 by enhancing light absorption. However, although the band gap can be continuously narrowed by pressure, the pressure-enhanced photocurrent saturates at approximately 17 GPa.

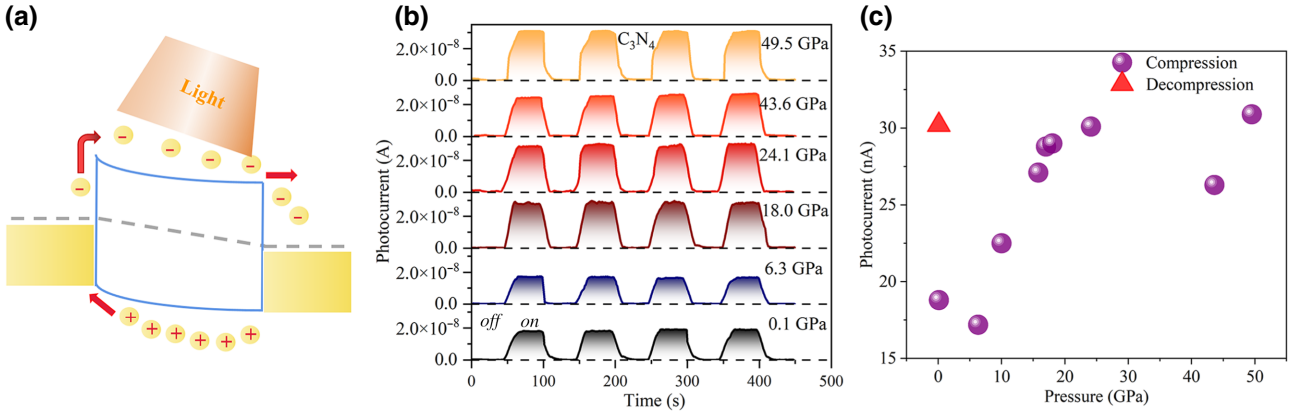

FIG. 4. Visible-light responsiveness of C_3N_4. (a) Schematic diagram of the photoconductive effect. (b) Photocurrent of C_3N_4 at selected pressures with a full spectrum of visible light at a 15-V bias. (c) Photocurrent as a function of pressure extracted from (b).

D. Pressure-induced amorphization of nitrogen-deficient g-C_3N_4 samples

To understand the pressure-modulated band gap and photocurrent, the structural evolution of nitrogen-deficient g-C_3N_4 under pressure is investigated by *in situ* Raman spectroscopy and synchrotron x-ray diffraction. A complete process of compressing and depressurizing nitrogen-deficient g-C_3N_4 is investigated by the Raman spectra depicted in Fig. 5(a). The Raman peak centered at about 1350 cm^{-1} represents the strong first-order Raman mode of the diamond anvil cell [63]. In the low-pressure region before 17 GPa, no Raman modes of nitrogen-deficient g-C_3N_4 can be found. Continuous compression results in the appearance of a broadened Raman band at approximately 1650 cm^{-1} [60]. In Fig. 5(b), the phonon frequencies of nitrogen-deficient g-C_3N_4 increase upon compression beyond 17 GPa, which is due to the shrinkage of the lattice or modulation of the crystal field by lattice distortion under pressure [64]. After depressurizing to 0 GPa, the Raman band moves to approximately 1620 cm^{-1}, which is near the earlier theoretical predictions of the C-N stretching model of g-C_3N_4 at approximately 1600 cm^{-1} under ambient conditions [14]. A similar broad Raman peak located at 1620 cm^{-1} is observed in the ultraviolet Raman spectrum of pristine g-C_3N_4. The broad Raman band decomposes into five peaks and is related to the coexistence of several polymorphs of g-C_3N_4 with different symmetries, and therefore, different Raman spectra [60]. The discrepancies in the phonon frequencies between compression and decompression suggest an irreversible structural phase transition at approximately 17 GPa.

As shown in Fig. 5(c), a comparative experiment under pressure is performed, in which the pressure of the sample increases from 0 to 15 GPa and then decreases back to 0 GPa. Subsequently, it is compressed to 48 GPa once again and finally returns to ambient conditions. The Raman spectrum at 0 GPa released from 15 GPa is similar to the spectrum before compression, and the characteristic peak of g-C_3N_4 near 1620 cm^{-1} cannot be observed. The results suggest that pressure leads to reversible elastic stretching of the lattice in nitrogen-deficient g-C_3N_4 before reaching 17 GPa and induces irreversible structural phase transitions at higher pressures.

To further investigate the origin of the irreversible structural phase transition, high-pressure synchrotron radiation is performed on nitrogen-deficient g-C_3N_4, as shown in Fig. 6. The synchrotron x-ray diffraction pattern of the nitrogen-deficient g-C_3N_4 sample before compression shows a clear (002) peak at $d = 3.18$ Å, which is consistent with the XRD result at ambient pressure in Fig. 1(a). Upon compression, the Bragg peaks associated with crystalline material disappear at 24.3 GPa, suggesting the formation of amorphization or disordering [65,66]. After depressurization to ambient pressure, amorphous g-C_3N_4 is retained with an XRD pattern similar to that at high pressure.

The Raman spectra and x-ray diffraction show coinciding evidence for an irreversible pressure-induced amorphization (PIA) at approximately 17 GPa for nitrogen-deficient g-C_3N_4. The crystalline structure of nitrogen-deficient g-C_3N_4 collapses upon compression, when the regular atomic arrangement is lost without sufficient thermal energy to achieve a more stable crystalline phase at temperatures far below the melting point or vitrification range [67,68]. Thus, before PIA, compression of the lattice notably narrows the band gap. With a further increase in pressure, the amorphized phase is less compressible than the crystalline phase and shows a slower rate for the pressure-narrowed band gap. For the photocurrent, although the narrowed band gap enhances light absorption, translational symmetry breaking in the amorphized phase reduces the charge mobility, which is averse to the photocurrent. As a result, the photocurrent is enhanced significantly upon compression before 17 GPa and almost does not change in the higher-pressure region. When the

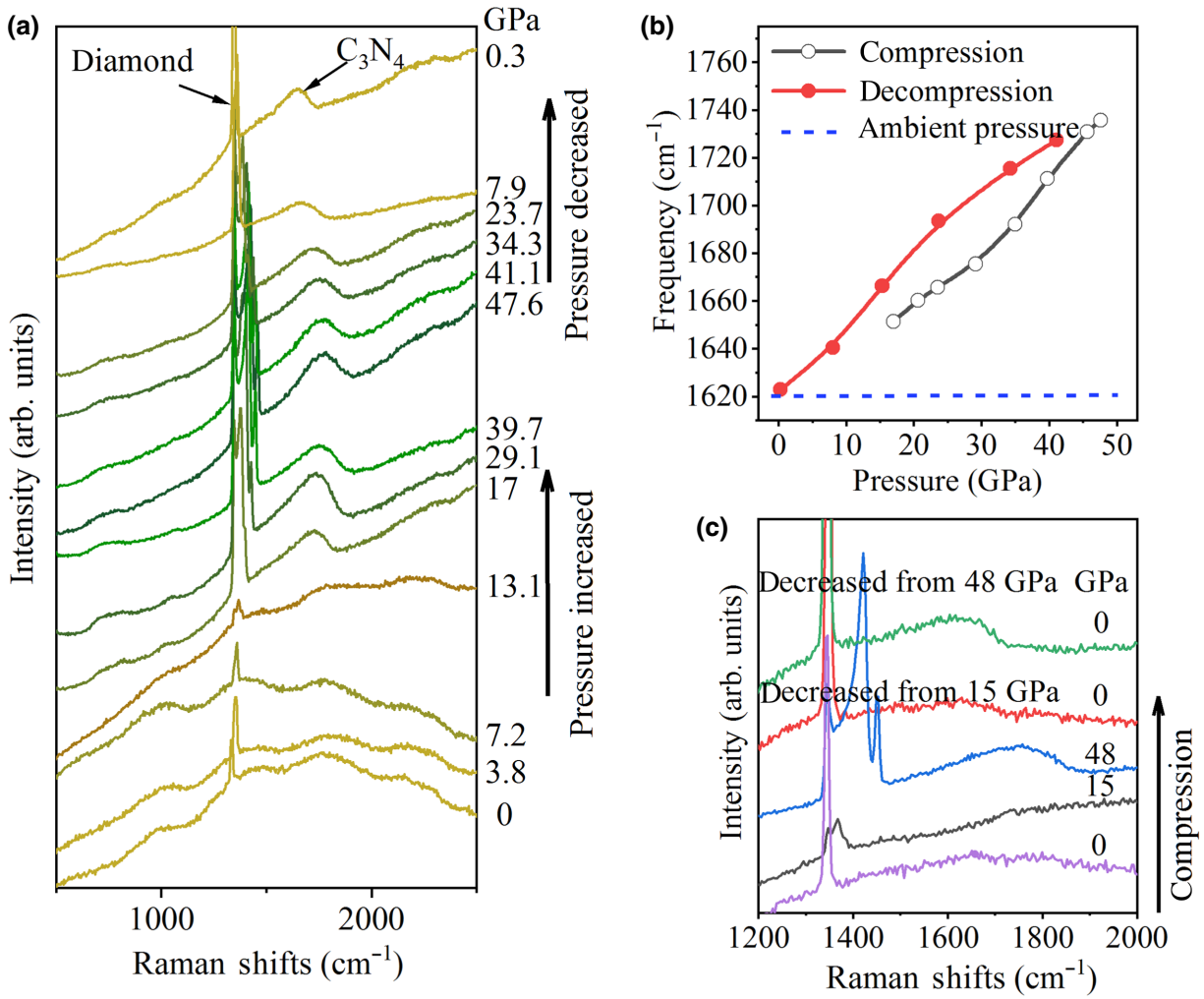

FIG. 5. Raman spectroscopy studies of nitrogen-deficient g-C_3N_4 under pressure. (a) Raman spectra of nitrogen-deficient g-C_3N_4 at high pressures. From bottom to top, it goes through the process of compression (from 0 to 47.6 GPa) and pressure relief (from 41.1 to 0.3 GPa). (b) Pressure-dependent phonon frequencies of nitrogen-deficient g-C_3N_4 during both compression and decompression processes. Blue dashed line represents the broad band centered at 1620 cm^{-1} at ambient pressure, as shown in Ref. [60]. (c) Representative Raman spectra at selected pressures. Sample reaches 15 GPa for the first compression and then unloads back to ambient pressure. With subsequent compression, the pressure increases up to 48 GPa and then depressurizes to zero.

pressure is released, the increased entropy in the amorphized phase due to the lack of long-range ordering prevents the dynamic instability-induced structural phase transition upon depressurization. The amorphized g-C_3N_4 has a narrowed band gap and enhanced photoelectric responsivity reserves at ambient pressure.

E. Discussion

The band structure determines the light-absorption ability and carrier-transport properties of the photocatalyst [69–71]. Narrowing the wide band gap of 2.70 eV in g-C_3N_4 is crucial to enhance its photocatalytic activity. The minimum band gap of undoped g-C_3N_4 reported in the literature is 1.90 eV in an amorphous sample prepared by annealing crystalline g-C_3N_4 at high temperature under an argon atmosphere [18]. An earlier optical investigation of g-C_3N_4 at high pressure successfully shifted the center wavelength of PL from blue to yellow. Here, a much lower band gap of 1.70 eV with red luminescence is achieved, as the initial nitrogen-deficient g-C_3N_4 has a lower band gap of 2.40 eV with yellow luminescence. As a result, the photoelectric response shows prominent enhancement near 50% under pressure. The higher photoelectric response will benefit its future applications as photodetectors in video imaging, optical communications, biomedical imaging, security, gas sensing, motion detection, and so on.

Intense interest in the synthesis of three-dimensional cubic C_3N_4 has been generated to secure superhard materials over the past few decades, as cubic C_3N_4 is predicted to have a zero-pressure bulk modulus exceeding

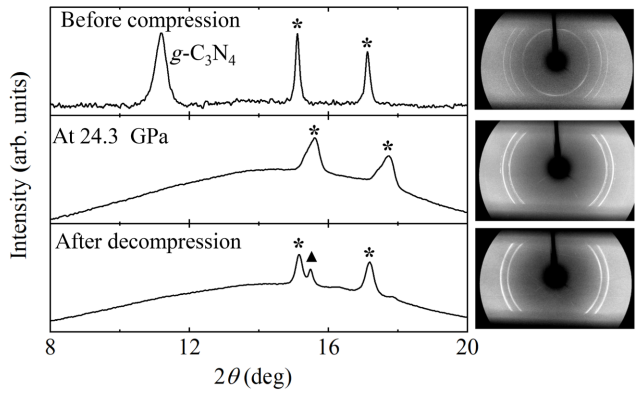

FIG. 6. Integrated synchrotron x-ray diffraction patterns and the corresponding two-dimensional XRD patterns. Stars (*) denote the diffraction peaks of Au, which are used to calibrate the pressure. Peak denoted by the triangle (▲) originates from the Re gasket.

that of diamond. Earlier first-principles studies predicted the transition from g-C_3N_4 to cubic C_3N_4 at approximately 12 GPa [52]. Lowther suggested a strong phase instability of the graphite structure without transformation to the cubic phase up to 60 GPa [53]. Although several works claim the synthesis of superhard C_3N_4 with nano- to microsizes under high-pressure and high-temperature conditions, revealing the high-pressure structural stability of C_3N_4 is still crucial to prepare macrosized cubic C_3N_4 with adequate structural characterization for more convincing evidence. Here, the transition from nitrogen-deficient g-C_3N_4 to the amorphous phase at 17 GPa is observed, which is in contrast with earlier theoretical calculations that the free energy of the amorphous phase is always higher than that of graphite phases up to 200 GPa [53]. Earlier structural characterization of pristine g-C_3N_4 at high pressure also did not report the PIA up to 125 GPa [72]. The discrepancy in pressure-induced phase transitions is probably because the initial g-C_3N_4 sample adopted here contains highly concentrated nitrogen vacancies with a N : C ratio of 9 : 10, while both the earlier theoretical calculations and experiments consider pristine g-C_3N_4 and overlook defects. The emergence of PIA with the assistance of nitrogen vacancies in C_3N_4 highlights the role of defects on the structural stability under pressure. Thus, to secure superhard C_3N_4 with a cubic structure, defects need to be involved in both theoretical calculations and experimental efforts.

Understanding and describing the structures and properties of amorphous states has long been a fundamental problem in condensed-matter physics. In general, the structural phase transition is determined by the total free energy: $G = U + PV - TS$, where U is internal energy, P is pressure applied, V is the volume, T is temperature, and S is the entropy. As the increase in internal energy, U, due to distortions necessary to destroy long-range order is higher than the decrease in G due to an increase in the entropy originating from the configurational disorder in the amorphous phase, the crystalline structure is usually more stable than the amorphous phase under ambient conditions. At high pressure, to achieve the lowest free energy, G, the equilibrium geometries transform either into a high-pressure crystalline phase by reducing the internal energy, U, or into an amorphous phase by increasing the entropy, S [67]. In the former case, atom-atom repulsions make the compression of volume resilient. Consequently, most of the pressure-driven crystalline-to-crystalline structural transitions are reversible, i.e., the high-pressure structure and physical properties usually cannot be achieved after depressurization to ambient pressure. On the other hand, the pressure decrease shows little influence on the entropy, S, increase due to the configurational disorder in the amorphous phase. As a result of the kinetic barrier, PIA is inclined to be irreversible [67]. Thus, using PIA to retain the high-pressure-optimized band gap and photoelectric response under ambient conditions can work in a variety of materials.

Although PIA is observed in a large number of materials, the apparently direct transformation to an amorphous phase below the melting point constitutes an open question with fundamental implications, as well as the opportunity to create amorphous materials [65,66]. Earlier investigations focused on the crystallography of PIA, and there is a lack of detailed studies on the optical and electric properties of the functional materials [67,68]. Here, the successful tuning of the band gap and photoelectric properties at ambient pressure in nitrogen-deficient g-C_3N_4 by PIA will aid efforts in band engineering of these materials. The defect-assisted PIA in nitrogen-deficient g-C_3N_4 implies that increasing structural instabilities, such as introducing vacancy defects, decreasing particle size, and increasing specific surface area, are likely to result in irreversible PIA in other materials that have not yet been observed [67]. We expect PIA to be adopted in a broad range of materials to engineer their optical and electrical properties for ambient-pressure applications.

IV. CONCLUSIONS

With the assistance of nitrogen vacancies, the PL of nitrogen-deficient g-C_3N_4 shifts from yellow to red upon compression with a minimum band gap of 1.70 eV at high pressure. The pressure-narrowed band gap enhances light absorption in the visible range and increases the photocurrent under white light from 18 to 29 nA. Moreover, irreversible pressure-induced amorphization appears at approximately 17.0 GPa. The narrowed band gap can be retained at ambient pressure when the applied pressure is higher than the PIA transition. Our results provide an insight into the structural stability and physical properties of g-C_3N_4. First, with the assistance of nitrogen

defects, the pressure-driven structural transformation from the graphitic phase to the amorphous phase is reported in C_3N_4, which highlights the role of defects in structural stability for the long-term securing of superhard cubic C_3N_4. Second, the minimum band gap of 1.70 eV at high pressure is smaller than the lowest value reported in the literature for undoped g-C_3N_4, illustrating the advantage of the high-pressure technique in tuning the band gap of semiconductors over a wide range. Third, the successful retention of the pressure-optimized band gap and photoelectric response after depressurization to 0 GPa supplies a strategy of vacancy-assisted PIA to engineer the band gap and photoelectric properties of broadened materials for various applications under ambient conditions.

ACKNOWLEDGMENTS

This work is supported by the National Natural Science Foundation of China (Grants No. 52002372, No. 51672279, and No. 51727806) and a CAS Innovation Grant (No. CXJJ-19-B08) and is carried out with support of the 4W2 beamline of the BSRF and the BL15U1 beamline of the SSRF.

The authors declare no competing financial interest.

[1] X. Wang, K. Maeda, A. Thomas, K. Takanabe, G. Xin, J. M. Carlsson, K. Domen, and M. Antonietti, A metal-free polymeric photocatalyst for hydrogen production from water under visible light, Nat. Mater. **8**, 76 (2009).

[2] Y. Wang, P. Du, H. Pan, L. Fu, Y. Zhang, J. Chen, Y. Du, N. Tang, and G. Liu, Increasing solar absorption of atomically thin 2D carbon nitride sheets for enhanced visible-light photocatalysis, Adv. Mater. **31**, e1807540 (2019).

[3] L. H. Lin, Z. Y. Lin, J. Zhang, X. Cai, W. Lin, Z. Y. Yu, and X. C. Wang, Molecular-level insights on the reactive facet of carbon nitride single crystals photocatalysing overall water splitting, Nat. Catal. **3**, 649 (2020).

[4] J. S. Zhang, M. Grzelczak, Y. D. Hou, K. Maeda, K. Domen, X. Z. Fu, M. Antonietti, and X. C. Wang, Photocatalytic oxidation of water by polymeric carbon nitride nanohybrids made of sustainable elements, Chem. Sci. **3**, 443 (2012).

[5] J. Liu, Y. Liu, N. Liu, Y. Han, X. Zhang, H. Huang, Y. Lifshitz, S. T. Lee, J. Zhong, and Z. Kang, Water splitting. Metal-free efficient photocatalyst for stable visible water splitting via a two-electron pathway, Science **347**, 970 (2015).

[6] F. Su, S. C. Mathew, G. Lipner, X. Fu, M. Antonietti, S. Blechert, and X. Wang, mpg-C_3N_4-catalyzed selective oxidation of alcohols using O_2 and visible light, J. Am. Chem. Soc. **132**, 16299 (2010).

[7] W. J. Ong, L. L. Tan, S. P. Chai, and S. T. Yong, Graphene oxide as a structure-directing agent for the two-dimensional interface engineering of sandwich-like graphene-g-C_3N_4 hybrid nanostructures with enhanced visible-light photoreduction of CO_2 to methane, Chem. Commun. **51**, 858 (2015).

[8] Q. Liu, F. Wang, Y. Jiang, W. Chen, R. Zou, J. Ma, L. Zhong, and X. Peng, Efficient photoreforming of lignocellulose into H_2 and photocatalytic CO_2 reduction via in-plane surface dyadic heterostructure of porous polymeric carbon nitride, Carbon **170**, 199 (2020).

[9] Y. Cui, Z. Ding, P. Liu, M. Antonietti, X. Fu, and X. Wang, Metal-free activation of H_2O_2 by g-C_3N_4 under visible light irradiation for the degradation of organic pollutants, Phys. Chem. Chem. Phys. **14**, 1455 (2012).

[10] S. Cao, J. Low, J. Yu, and M. Jaroniec, Polymeric photocatalysts based on graphitic carbon nitride, Adv. Mater. **27**, 2150 (2015).

[11] Y. Wang, X. Wang, and M. Antonietti, Polymeric graphitic carbon nitride as a heterogeneous organocatalyst: From photochemistry to multipurpose catalysis to sustainable chemistry, Angew. Chem., Int. Ed. **51**, 68 (2012).

[12] L. S. Zhang, N. Ding, M. Hashimoto, K. Iwasaki, N. Chikamori, K. Nakata, Y. Z. Xu, J. J. Shi, H. J. Wu, Y. H. Luo, *et al.*, Sodium-doped carbon nitride nanotubes for efficient visible light-driven hydrogen production, Nano Res. **11**, 2295 (2018).

[13] Z. Fu, Z. Ma, T. Yu, and L. Bi, A first blue fluorescence composite film based on graphitic carbon nitride nanosheets/polyoxometalate for application in reversible electroluminescence switching, J. Mater. Chem. C **7**, 3253 (2019).

[14] T. Suter, V. Brázdová, K. McColl, T. S. Miller, H. Nagashima, E. Salvadori, A. Sella, C. A. Howard, C. W. M. Kay, F. Corà, *et al.*, Synthesis, structure and electronic properties of graphitic carbon nitride films, J. Phys. Chem. C **122**, 25183 (2018).

[15] H. Wang, S. Min, C. Ma, Z. Liu, W. Zhang, Q. Wang, D. Li, Y. Li, S. Turner, Y. Han, *et al.*, Synthesis of single-crystal-like nanoporous carbon membranes and their application in overall water splitting, Nat. Commun. **8**, 13592 (2017).

[16] J. Wang, Y. Li, L. Deng, N. Wei, Y. Weng, S. Dong, D. Qi, J. Qiu, X. Chen, and T. Wu, High-performance photothermal conversion of narrow-bandgap Ti_2O_3 nanoparticles, Adv. Mater. **29**, 1603730 (2017).

[17] Y. Y. Li, Y. Yan, X. Y. Shu, D. Y. Wang, N. N. Wei, X. J. Yu, M. B. H. Breese, T. Venkatesan, J. M. Xue, Y. C. Liu, *et al.*, From titanium sesquioxide to titanium dioxide: Oxidation-induced structural, phase, and property evolution, Chem. Mater. **30**, 4383 (2018).

[18] Y. Kang, Y. Yang, L. C. Yin, X. Kang, G. Liu, and H. M. Cheng, An amorphous carbon nitride photocatalyst with greatly extended visible-light-responsive range for photocatalytic hydrogen generation, Adv. Mater. **27**, 4572 (2015).

[19] P. Niu, L. C. Yin, Y. Q. Yang, G. Liu, and H. M. Cheng, Increasing the visible light absorption of graphitic carbon nitride (melon) photocatalysts by homogeneous self-modification with nitrogen vacancies, Adv. Mater. **26**, 8046 (2014).

[20] A. H. Proppe, Y. G. C. Li, A. Aspuru-Guzik, C. P. Berlinguette, C. J. Chang, R. Cogdell, A. G. Doyle, J. Flick, N. M. Gabor, R. van Grondelle, *et al.*, Bioinspiration in light harvesting and catalysis, Nat. Rev. Mater. **5**, 828 (2020).

[21] J. Zhang, M. Deng, Y. Yan, T. Xiao, W. Ren, and P. Zhang, Tunable Type-II $BiVO_4/g\text{-}C_3N_4$ Nanoheterostructures for Photocatalysis Applications, Phys. Rev. Appl. **11**, 044052 (2019).

[22] Z. Lin and X. Wang, Nanostructure engineering and doping of conjugated carbon nitride semiconductors for hydrogen photosynthesis, Angew. Chem., Int. Ed. **52**, 1735 (2013).

[23] G. Liu, P. Niu, C. Sun, S. C. Smith, Z. Chen, G. Q. Lu, and H. M. Cheng, Unique electronic structure induced high photoreactivity of sulfur-doped graphitic C_3N_4, J. Am. Chem. Soc. **132**, 11642 (2010).

[24] J. S. Zhang, J. H. Sun, K. Maeda, K. Domen, P. Liu, M. Antonietti, X. Z. Fu, and X. C. Wang, Sulfur-mediated synthesis of carbon nitride: Band-gap engineering and improved functions for photocatalysis, Energy Environ. Sci. **4**, 675 (2011).

[25] J. Li, B. Shen, Z. Hong, B. Lin, B. Gao, and Y. Chen, A facile approach to synthesize novel oxygen-doped $g\text{-}C_3N_4$ with superior visible-light photoreactivity, Chem. Commun. **48**, 12017 (2012).

[26] Y. Zhang, T. Mori, J. Ye, and M. Antonietti, Phosphorus-doped carbon nitride solid: Enhanced electrical conductivity and photocurrent generation, J. Am. Chem. Soc. **132**, 6294 (2010).

[27] J. Xu, Y. Li, S. Peng, G. Lu, and S. Li, Eosin Y-sensitized graphitic carbon nitride fabricated by heating urea for visible light photocatalytic hydrogen evolution: The effect of the pyrolysis temperature of urea, Phys. Chem. Chem. Phys. **15**, 7657 (2013).

[28] S. X. Min and G. X. Lu, Enhanced electron transfer from the excited Eosin Y to mpg-C_3N_4 for highly efficient hydrogen evolution under 550 nm irradiation, J. Phys. Chem. C **116**, 19644 (2012).

[29] H. Yu, R. Shi, Y. Zhao, T. Bian, Y. Zhao, C. Zhou, G. I. N. Waterhouse, L. Z. Wu, C. H. Tung, and T. Zhang, Alkali-assisted synthesis of nitrogen deficient graphitic carbon nitride with tunable band structures for efficient visible-light-driven hydrogen evolution, Adv. Mater. **29**, 1605148 (2017).

[30] Z. Hong, B. Shen, Y. Chen, B. Lin, and B. Gao, Enhancement of photocatalytic H_2 evolution over nitrogen-deficient graphitic carbon nitride, J. Mater. Chem. A **1**, 11754 (2013).

[31] P. Niu, G. Liu, and H. M. Cheng, Nitrogen vacancy-promoted photocatalytic activity of graphitic carbon nitride, J. Phys. Chem. C **116**, 11013 (2012).

[32] W. Tu, Y. Xu, J. Wang, B. Zhang, T. Zhou, S. Yin, S. Wu, C. Li, Y. Huang, Y. Zhou, *et al.*, Investigating the role of tunable nitrogen vacancies in graphitic carbon nitride nanosheets for efficient visible-light-driven H_2 evolution and CO_2 reduction, ACS Sustainable Chem. Eng. **5**, 7260 (2017).

[33] J. J. Wu, N. Li, H. B. Fang, X. T. Li, Y. Z. Zheng, and X. Tao, Nitrogen vacancies modified graphitic carbon nitride: Scalable and one-step fabrication with efficient visible-light-driven hydrogen evolution, Chem. Eng. J. **358**, 20 (2019).

[34] J. Liao, W. Cui, J. Li, J. Sheng, H. Wang, X. A. Dong, P. Chen, G. Jiang, Z. Wang, and F. Dong, Nitrogen defect structure and NO^+ intermediate promoted photocatalytic NO removal on H_2 treated $g\text{-}C_3N_4$, Chem. Eng. J. **379**, 122282 (2020).

[35] L. J. Zhang, Y. C. Wang, J. Lv, and Y. M. Ma, Materials discovery at high pressures, Nat. Rev. Mater. **2**, 17005 (2017).

[36] J. Shi, W. Cui, J. Hao, M. Xu, X. Wang, and Y. Li, Formation of ammonia-helium compounds at high pressure, Nat. Commun. **11**, 3164 (2020).

[37] Z. Y. Cao, J. W. Hu, A. F. Goncharov, and X. J. Chen, Nontrivial metallic state of MoS_2, Phys. Rev. B **97**, 214519 (2018).

[38] P. Cheng, X. Yang, X. Zhang, Y. Wang, S. Jiang, and A. F. Goncharov, Polymorphism of polymeric nitrogen at high pressures, J. Chem. Phys. **152**, 244502 (2020).

[39] A. Jayaraman, Diamond anvil cell and high-pressure physical investigations, Rev. Mod. Phys. **55**, 65 (1983).

[40] E. Horvath-Bordon, R. Riedel, A. Zerr, P. F. McMillan, G. Auffermann, Y. Prots, W. Bronger, R. Kniep, and P. Kroll, High-pressure chemistry of nitride-based materials, Chem. Soc. Rev. **35**, 987 (2006).

[41] L. C. Ming, P. Zinin, Y. Meng, X. R. Liu, S. M. Hong, and Y. Xie, A cubic phase of C_3N_4 synthesized in the diamond-anvil cell, J. Appl. Phys. **99**, 033520 (2006).

[42] V. Schettino and R. Bini, Constraining molecules at the closest approach: Chemistry at high pressure, Chem. Soc. Rev. **36**, 869 (2007).

[43] P. Jing, D. Han, D. Li, D. Zhou, D. Shen, G. Xiao, B. Zou, and S. Qu, Surface related intrinsic luminescence from carbon nanodots: Solvent dependent piezochromism, Nanoscale Horiz. **4**, 175 (2019).

[44] B. Szentpeteri, P. Rickhaus, F. K. de Vries, A. Marffy, B. Fulop, E. Tovari, K. Watanabe, T. Taniguchi, A. Kormanyos, S. Csonka, *et al.*, Tailoring the band structure of twisted double bilayer graphene with pressure, Nano Lett. **21**, 8777 (2021).

[45] M. Yankowitz, S. Chen, H. Polshyn, Y. Zhang, K. Watanabe, T. Taniguchi, D. Graf, A. F. Young, and C. R. Dean, Tuning superconductivity in twisted bilayer graphene, Science **363**, 1059 (2019).

[46] T. Ye, P. Cheng, H. Zeng, D. Yao, X. Pan, H. Jiang, and J. Ding, Pressure-induced bifurcation in the photoluminescence of red carbon quantum dots: Coexistence of emissions from surface groups and nitrogen-doped cores, J. Phys. Chem. Lett. **13**, 4768 (2022).

[47] Q. Li, L. Zhang, Z. Chen, and Z. Quan, Metal halide perovskites under compression, J. Mater. Chem. A **7**, 16089 (2019).

[48] Q. Li, Z. Chen, B. Yang, L. Tan, B. Xu, J. Han, Y. Zhao, J. Tang, and Z. Quan, Pressure-induced remarkable enhancement of self-trapped exciton emission in one-dimensional $CsCu_2I_3$ with tetrahedral units, J. Am. Chem. Soc. **142**, 1786 (2020).

[49] Q. Li, H. Cheng, C. Xing, S. Guo, X. Wu, L. Zhang, D. Zhang, X. Liu, X. Wen, X. Lu, *et al.*, Pressure-induced amorphization and crystallization of heterophase Pd nanostructures, Small **18**, e2106396 (2022).

[50] N. Gross, Y.-Y. Sun, S. Perera, H. Hui, X. Wei, S. Zhang, H. Zeng, and B. A. Weinstein, Stability and Band-Gap Tuning of the Chalcogenide Perovskite $BaZrS_3$ in Raman and

Optical Investigations at High Pressures, Phys. Rev. Appl. **8**, 044014 (2017).

[51] G. Liu, L. P. Kong, J. Gong, W. G. Yang, H. K. Mao, Q. Y. Hu, Z. X. Liu, R. D. Schaller, D. Z. Zhang, and T. Xu, Pressure-induced bandgap optimization in lead-based perovskites with prolonged carrier lifetime and ambient retainability, Adv. Funct. Mater. **27**, 1604208 (2017).

[52] D. M. Teter and R. J. Hemley, Low-compressibility carbon nitrides, Science **271**, 53 (1996).

[53] J. E. Lowther, Relative stability of some possible phases of graphitic carbon nitride, Phys. Rev. B **59**, 11683 (1999).

[54] L. M. Fang, H. Ohfuji, T. Shinmei, and T. Irifune, Experimental study on the stability of graphitic C_3N_4 under high pressure and high temperature, Diamond Relat. Mater. **20**, 819 (2011).

[55] K. Hu, M. Yao, Z. Yang, G. Xiao, L. Zhu, H. Zhang, R. Liu, B. Zou, and B. Liu, Pressure tuned photoluminescence and band gap in two-dimensional layered g-C_3N_4: The effect of interlayer interactions, Nanoscale **12**, 12300 (2020).

[56] J. Ding, P. Cheng, T. Ye, W. Xu, H. Zeng, D. Yao, X. Pan, and J. Zhang, Pressure-induced two-dimensional to three-dimensional structural phase transition in $2H$-type layered lead iodide PbI_2, Appl. Phys. Lett. **120**, 052106 (2022).

[57] A. P. Hammersley, S. O. Svensson, M. Hanfland, A. N. Fitch, and D. Hausermann, Two-dimensional detector software: From real detector to idealised image or two-theta scan, High Pressure Res. **14**, 235 (1996).

[58] J. F. Ding, T. T. Ye, H. C. Zhang, X. Yang, H. Zeng, C. G. Zhang, and X. L. Wang, Pressure-induced structural phase transition and vacancy filling in titanium monoxide TiO up to 50 GPa, Appl. Phys. Lett. **115**, 101902 (2019).

[59] F. Fina, S. K. Callear, G. M. Carins, and J. T. S. Irvine, Structural investigation of graphitic carbon nitride via XRD and neutron diffraction, Chem. Mater. **27**, 2612 (2015).

[60] P. V. Zinin, L. C. Ming, S. K. Sharma, V. N. Khabashesku, X. R. Liu, S. M. Hong, S. Endo, and T. Acosta, Ultraviolet and near-infrared Raman spectroscopy of graphitic C_3N_4 phase, Chem. Phys. Lett. **472**, 69 (2009).

[61] See the Supplemental Material at http://link.aps.org/supplemental/10.1103/PhysRevApplied.19.024048 for details about the XPS full spectrum, the color change of the sample, the I-V curve, and photocurrent curves before compression and after decompression.

[62] Z. J. Xie, Y. P. Feng, F. L. Wang, D. N. Chen, Q. X. Zhang, Y. Q. Zeng, W. Y. Lv, and G. G. Liu, Construction of carbon dots modified MoO_3/g-C_3N_4 Z-scheme photocatalyst with enhanced visible-light photocatalytic activity for the degradation of tetracycline, Appl. Catal., B **229**, 96 (2018).

[63] H. K. Mao, X. J. Chen, Y. Ding, B. Li, and L. Wang, Solids, liquids, and gases under high pressure, Rev. Mod. Phys. **90**, 015007 (2018).

[64] D. Pan and G. Galli, A first principles method to determine speciation of carbonates in supercritical water, Nat. Commun. **11**, 421 (2020).

[65] S. K. Deb, M. Wilding, M. Somayazulu, and P. F. McMillan, Pressure-induced amorphization and an amorphous-amorphous transition in densified porous silicon, Nature **414**, 528 (2001).

[66] H. Xiong, H. Yildirim, P. Podsiadlo, J. Zhang, V. B. Prakapenka, J. P. Greeley, E. V. Shevchenko, K. K. Zhuravlev, S. Tkachev, S. K. Sankaranarayanan, *et al.*, Compositional Tuning of Structural Stability of Lithiated Cubic Titania via a Vacancy-Filling Mechanism under High Pressure, Phys. Rev. Lett. **110**, 078304 (2013).

[67] D. Machon, F. Meersman, M. C. Wilding, M. Wilson, and P. F. McMillan, Pressure-induced amorphization and polyamorphism: Inorganic and biochemical systems, Prog. Mater Sci. **61**, 216 (2014).

[68] S. M. Sharma and S. K. Sikka, Pressure induced amorphization of materials, Prog. Mater Sci. **40**, 1 (1996).

[69] L. Cheng, Q. J. Xiang, Y. L. Liao, and H. W. Zhang, CdS-based photocatalysts, Energy Environ. Sci. **11**, 1362 (2018).

[70] J. Tang, Z. Zou, and J. Ye, Efficient photocatalytic decomposition of organic contaminants over $CaBi_2O_4$ under visible-light irradiation, Angew. Chem., Int. Ed. **43**, 4463 (2004).

[71] H. J. Zhang, G. H. Chen, and D. W. Bahnemann, Photoelectrocatalytic materials for environmental applications, J. Mater. Chem. **19**, 5089 (2009).

[72] Y. Kojima and H. Ohfuji, Structure and stability of carbon nitride under high pressure and high temperature up to 125 GPa and 3000 K, Diamond Relat. Mater. **39**, 1 (2013).